Electronic origin of spatial self-phase modulation: Evidenced by comparing graphite with C60 and graphene

Y. L. Wu, L. L. Zhu, Q. Wu, F. Sun, J. K. Wei, Y. C. Tian, W. L. Wang, X. D. Bai, Xu Zuo, and Jimin Zhao

Citation: Applied Physics Letters **108**, 241110 (2016); doi: 10.1063/1.4953827
View online: http://dx.doi.org/10.1063/1.4953827
View Table of Contents: http://scitation.aip.org/content/aip/journal/apl/108/24?ver=pdfcov
Published by the AIP Publishing

APPLIED PHYSICS LETTERS **108**, 241110 (2016)

Electronic origin of spatial self-phase modulation: Evidenced by comparing graphite with C_{60} and graphene

Y. L. Wu,[1,2] L. L. Zhu,[1,2] Q. Wu,[2] F. Sun,[2] J. K. Wei,[2] Y. C. Tian,[2] W. L. Wang,[2] X. D. Bai,[2] Xu Zuo,[1,a)] and Jimin Zhao[2,a)]
[1]*College of Electronic Information and Optical Engineering, Nankai University, Tianjin 300071, China*
[2]*Beijing National Laboratory for Condensed Matter Physics and Institute of Physics, Chinese Academy of Sciences, Beijing 100190, China*

(Received 3 February 2016; accepted 1 June 2016; published online 16 June 2016)

We report unambiguous observation of spatial self-phase modulation (SSPM) in a dispersive suspension of graphite flakes. This coherent nonlinear optical effect in bulk graphite is found to be broadband and large, with a third-order nonlinear susceptibility $\chi^{(3)}$ of 2.2×10^{-9} esu (i.e., 3.1×10^{-17} m^2/V^2 in SI units) at 532 nm excitation. Comparison with other carbon allotropes shows that this value is 5×10^7 times higher than that of C_{60} but $\sim$50 times lower than that of graphene, fully exhibiting the electronic origin of SSPM. *Published by AIP Publishing.* [http://dx.doi.org/10.1063/1.4953827]

Spatial self-phase modulation (SSPM) is a coherent third-order nonlinear optical effect, which was investigated in nematic-liquid-crystal decades ago.[1] Thereafter, various materials have been found preserving this property, especially the recently discovered two-dimensional (2D) quantum materials[2–5] such as MoS_2,[6] graphene,[7] and $MoSe_2$.[8] These layered electronic materials have relatively high photo-carrier mobilities, leading to relatively higher nonlinear optical response $\chi^{(3)}$ values, which are fundamentally determined by their band structures. Here, we particularly investigate and compare the SSPM properties of various forms of carbon materials. It has been found that the $\chi^{(3)}$ values for the zero-dimensional (0D) C_{60} (1.8×10^{-12} esu for 15 mg/l),[9,10] one-dimensional (1D) carbon nanotube (10^{-11}–10^{-14} esu for 80 or 330 mg/l),[11,12] and 2D graphene (1.0×10^{-7} esu for effective one-layer or equivalently 0.075 mg/l)[7] are largely different. The small value for the 1D carbon nanotubes can be ascribed to impure samples due to the mixing between metallic and semiconducting tubes. However, it is necessary to clarify why the 0D C_{60} and 2D graphene have so much different values of $\chi^{(3)}$. By obtaining the $\chi^{(3)}$ value for graphite, a three-dimensional (3D) allotrope of carbon, we ascribe it to the correlation between the value of $\chi^{(3)}$ and the capability of carrier motion in the material—an electronic property rather than a thermal property.

Unlike other optical properties that require broken spatial inversion symmetry,[13–16] heterojunction,[17] or heterogeneity,[18] the SSPM is demonstrated to be a ubiquitous property existing in most of the layered quantum materials.[6–8] The SSPM is characterized by a nonlinear refractive index $n = n_0 + n_2 I$, where n_0 and n_2 are linear and nonlinear refractive indices and I is the laser intensity. Brief introductions about SSPM are given in Refs. 6–8. A set of out-going conical diffraction beams form interference fringes at a far field screen. The ring number N is linearly dependent on the laser intensity and is proportional to the acquired optical phase owing to the transverse gradient in refractive index. There is a one-to-one correspondence between n_2 and $\chi^{(3)}$, both of which can be conveniently obtained by measuring the linear dependence of N on laser fluence.[6–8] The SSPM is also referred to as the optical Kerr effect (or, ac Kerr effect), by which, ac electron coherence (i.e., the electron wave function preserves well-defined phase) can be induced.[6] In addition, as shown in Ref. 6, a weak-control-strong,[19] cascade-possible, high-contrast-ratio all-optical switching based on SSPM has been achieved by tuning the ring diameter D. Thus, our current investigation endows graphite potential for photonics applications.

In graphite, the carbon atoms are sp^2 hybridized and electron hopping is confined in a 2D graphene-like layer. Due to similar chemical bond and energy band structure[20–23] to those of graphene, a relatively large $\chi^{(3)}$ nonlinearity is expected, which nonetheless may be alleviated by inter-layer interactions. In a polycrystalline graphite, restrictions of domain boundaries are expected to further reduce the value of $\chi^{(3)}$, owing to their non-coherent nature. On the other hand, an apparent difference between graphite flakes and C_{60} is their sizes. Unlike in graphite flakes, in C_{60} electron hoping is refrained within a small volume. Although this small volume will not necessarily affect too much the thermal effect, the limited dimension together with the non-layered structure restricts in-plane motion of free quasiparticles including electrons, holes, and excitons.

In this work, we directly measure the $\chi^{(3)}$ value of graphite and compare it with those of other carbon allotropes. The measured value is much larger than that of C_{60} and noticeably smaller than that of graphene, which both confirm that the SSPM formation is more likely an electronic property, rather than a thermal property. Such comparison between carbon allotropies helps understanding the SSPM formation mechanism.

Dispersive suspensions of graphite flakes in *N*-methyl-2-pyrrolidinone (NMP) solvent were prepared. Graphite flakes at various lateral sizes were investigated—in four different samples, marked by α, β, γ, and δ (Fig. 1(a)). The nominal sizes

[a)]Authors to whom correspondence should be addressed. Electronic addresses: jmzhao@iphy.ac.cn and xzuonku@outlook.com

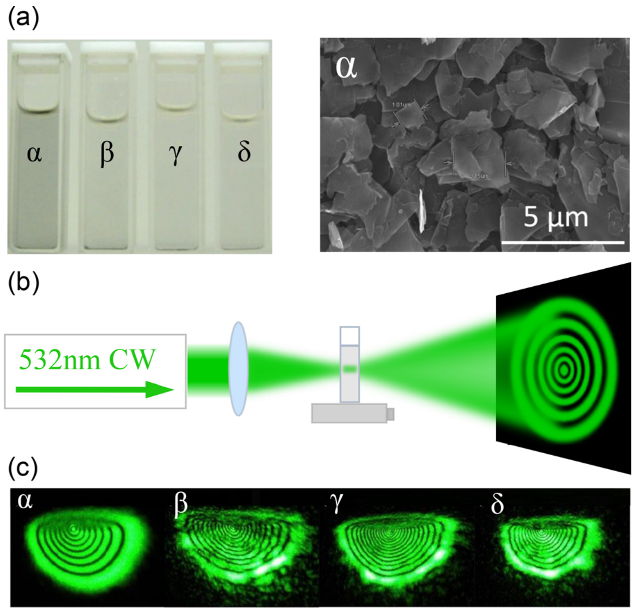

FIG. 1. (a) Photographs of four different samples (with different flake sizes) and the SEM image of sample α. (b) Schematic experimental setup. (c) SSPM patterns for the four samples.

are: α, 1 μm (nature, 99.9%); β, 2–15 μm (nature, 99.9995%); γ, 7–10 μm (nature, 99%); and δ, 44 μm (synthetic, 99.9995%). The graphite flakes for α were purchased from the Lacey City Shuangxing Graphite Processing Plant in Qingdao (http://sxliujingwen.en.b2b168.com/), and those for β, γ, and δ were purchased from Alfa Aesar, Inc. The containers are 10-mm-thick cuvettes, and the samples were sonicated for 30 min right before the experiments. The schematic setup is shown in Fig. 1(b), where a linearly polarized continuous wave laser beam is focused onto the graphite suspension by a lens of 200 mm focal length. The distance between the lens and the center of the cuvette is 154 mm. The $1/e^2$ intensity radius at the center of the cuvette is 0.199 mm for 532 nm beam and 0.241 mm for 473 nm beam, respectively. The nonlinear SSPM diffraction rings were clearly observed on a white screen placed 3.3 m away.

The photographs of patterns are shown in Fig.1(c). During the experiment, it was found that larger size flakes (those for β, γ, and δ) are easier to precipitate to the bottom of the cuvette (see Fig. 1(a)), which are accompanied by relatively unstable ring patterns on the screen (see Fig. 1(c)). This demonstrates that the maximum flake size for a practical sample is roughly that for sample α. To unambiguously see the flake size in sample α, we performed scanning electron microscope (SEM) characterization right after the SSPM experiment. The flakes were collected after vaporization of the solution. As shown in Fig. 1(a), the lateral size has a distribution of 0.5 – 4 μm. Also, clear diffraction rings are essential for the measurements. Thus, from Fig. 1(c), we chose sample α to do the SSPM experiment. We have performed control experiment on pure NMP without any flakes, where no SSPM effect was observed at even very high laser fluence.

It is essential to verify that our sample composes of 3D graphite instead of 2D graphene. Because SEM is unable to identify monolayer or few-layer graphene, we further performed tunneling electron microscope (TEM), Raman scattering, and X-ray diffraction (XRD). In Figs. 2(a) and 2(b), the high resolution TEM image of flakes in sample α shows that the thickness of a randomly selected flake is about 7 nm or 20 layers. We characterized 10 sample positions on different flakes, where the thickness ranges from 3 nm to 15 nm, corresponding to 9–45 layers. Besides, no single-layer graphene was observed.

In Fig. 2(c), we show a Raman spectrum of the flakes in sample α, which reveals the 3D crystallographic nature of the flakes. For sp^2 hybridized carbon lattices, the first-order Raman G peak is at 1560 cm^{-1} and the D peak is at 1350 cm^{-1} for visible excitation. The second-order 2D peak is at $\sim$2700 cm^{-1}, and another second-order intra-valley 2D$'$ peak is at $\sim$3250 cm^{-1}. Generally, we distinguish graphene and bulk graphite by the relative intensity between the G and 2D peaks and the shape of 2D peak, both of which are sensitive to the number of graphene layers.[24,25] The intensity of G peak increases nearly linearly with increasing layer number from 1 to 20, and its intensity is weaker than that of 2D when the layer number is less than 5.[24] Shown in Fig. 2(c), the relative intensity of G peak over 2D peak is higher than that for the graphene case.[7] Also, the shape of the 2D peak tends to become asymmetric and split into two peaks with increasing layer number.[25] Figure 2(c) shows that the 2D peak is noticeably asymmetric. Therefore for both features, our Raman characterization exhibits signatures of bulk graphite.

In Fig. 2(d), we present the XRD pattern of sample α. Generally, the (101) and (100) peaks become weaker with decreasing layer number and vanish for graphene.[26–30] In Fig. 2(d), they can be clearly identified. Furthermore, it is known the (002) peak is symmetric for graphite but asymmetric for single- and few-layer graphene.[28] As shown in Fig. 2(d), the (002) peak is fully symmetric, which is quite different from the asymmetric case for multi-layer graphene.[29] In addition, the angle value for the (002) peak illustrates the interlayer distance between parallel graphene layers.[30] In our experiment,

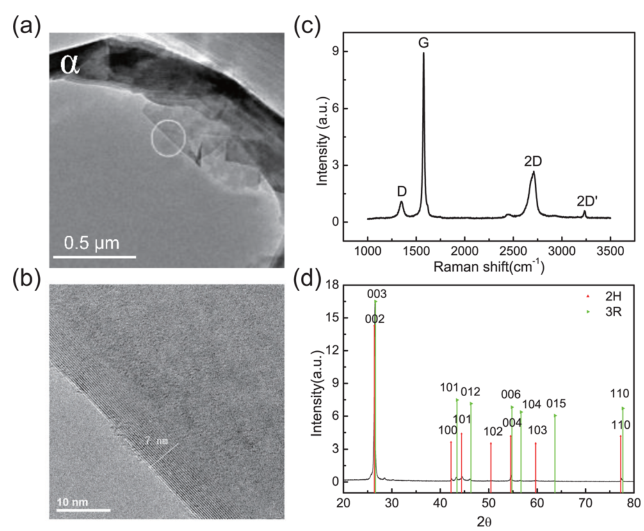

FIG. 2. Characterizations of the flakes in sample α. (a) The TEM image, where the small white circle indicates the flake edge, whose high resolution TEM (b) reveals the thickness of the flake. (c) Raman spectra. (d) X-ray diffraction pattern. The red and green lines indicate the 2H and 3R stacking patterns, respectively, demonstrating the coexistence of both hexagonal and trigonal stackings.

the angle value for the (002) peak is 26.48°, which corresponds to an interlayer distance of 0.336 nm. This is nearly identical to that for bulk graphite, 0.335 nm.[31] Thus, from the above TEM, Raman, and XRD characterizations, we can claim that our sample is bulk graphite flakes rather than single- or few-layer graphene.

Obtaining the third-order nonlinear susceptibility $\chi^{(3)}$ by using SSPM is straightforward, by recording the number of fringes. The phase accumulation $\Delta\psi$ of a laser beam after traversing the medium of thickness l is $\Delta\psi(r) = \frac{2\pi n_0}{\lambda}\int_{-l/2}^{l/2} n_2 I(r,z)dz$, where l is the sample thickness (involved in the SSPM) and z is the propagation direction of the incident beam. The number of rings N is proportional to the phase change in the output beam $\Delta\psi(0) - \Delta\psi(\infty) = 2\pi N$. For a Gaussian beam, $\Delta\psi(r) \approx \Delta\psi_0 \exp(-2r^2/a^2)$, where a is the $1/e^2$ beam intensity radius. With $I(0, z) = 2I$, we derive from $2\pi N = (2\pi n_0/\lambda)n_2 \cdot 2I \cdot l$ that $n_2 = (\lambda/2n_0 l)(N/I)$. Note that the term on the right side can be measured in the experiments. In Fig. 3(a), taking $l = 10$ mm and $n_0 = 1.47$ (for NMP solvent), we obtained $n_2 = 2.32 \times 10^{-10}$ (m^2/W) for 532 nm and $n_2 = 3.02 \times 10^{-10}$ (m^2/W) for 473 nm, respectively. Since the value of $\chi^{(3)}$ is one-to-one correspondent to the value of n_2, with $n_2 = (12\pi^2/(n_0{}^2 c))10^3\chi^{(3)}$ (in the SI unit),[7] we estimate that $\chi^{(3)}_{\text{total}} = 1.27 \times 10^{-4}$ esu (for 532 nm) and $\chi^{(3)}_{\text{total}} = 1.65 \times 10^{-4}$ esu (for 473 nm), respectively.

To derive the $\chi^{(3)}$ value for a single effective layer, the number of effective layers passed through by the laser beam was estimated. The volume of the solution sample is $V = 4 \times 10^{-3}$ l, which contains 0.072 mg graphite flakes without precipitation. Thus, the total number of carbon atoms is $M = 3.612 \times 10^{18}$. Due to the C–C bond distance 1.42 Å for graphite, the area A of a single regular hexagon is 5.24 Å^2, which contains equivalently two carbon atoms. The cross-section area S of the cuvette containing sample, which is normal to the light propagation direction, is 4 cm^2. Therefore, a single effective layer contains $m = 2S/A = 2 \times 4\,\text{cm}^2/5.24\,\text{Å}^2 = 1.5 \times 10^{16}$ carbon atoms. Hence, the effective layer number is $N = M/m = 240$. Due to the coherent behavior of SSPM, the far field fringes are a result of constructive interference of each composing effective one layer. So, we have $I_{\text{total}} \approx N^2 I_{\text{one layer}}$. Therefore, we estimate that $\chi^{(3)}_{\text{total}} = N^2 \chi^{(3)}_{\text{one layer}}$, and deduce that $\chi^{(3)}_{\text{one layer}}$ (equivalent to 0.075 mg/l in our experiment) to be 2.2×10^{-9} esu (i.e., 3.1×10^{-17} m^2/V^2) for 532 nm and 2.9×10^{-9} esu (i.e., 4.0×10^{-17} m^2/V^2) for 473 nm. A general comparison with other carbon materials is summarized in a table in the supplementary material.[32]

The above value is much higher than that of 0D C_{60} (in the comparable way, 5×10^7 times larger), which demonstrates that the formation of SSPM pattern is of electronic origin rather than of a thermal effect. The absorbances of the two materials are not so much different. What is different is that photo-carriers can move freely in graphite, but not in the C_{60} materials due to the small size of the molecule. In parallel, compared with graphene, real graphite flakes are all composed of poly-crystallines and electrons therein inevitably experience much more scatterings and reflections at the domain boundaries and defects. This will reduce the $\chi^{(3)}_{\text{one layer}}$ value for the electronic origin but not for the thermal (absorption) origin. Hence, if electronic origin is valid, graphite has apparent smaller $\chi^{(3)}$ than graphene. In contrast, if thermal origin is true, no apparent difference between graphite and graphene is expected. In our experiment, the value of effective one-layer $\chi^{(3)}$ is prominently $\sim$50 times smaller than that of graphene, which strongly supports the mechanism of electronic origin.

We then recorded the SSPM pattern formation process. Shown in the snapshots in Fig. 3(b), the rings are full circles without deformation and N increases steadily with time. According to the wind chime model,[6] the flakes are aligned by the light field and the electron coherence are induced by the incident light.[6] It takes about 0.4 s for the fringes to form. Quantitatively, we estimate the pattern formation time $\mathcal{T}$ by[6]

$$\mathcal{T} = \frac{\varepsilon_r \pi \eta \xi R c}{1.72(\varepsilon_r - 1)Ih} \approx 0.43\,\text{s}, \quad (1)$$

where the dielectric constant of graphite ε_r is estimated to be 13, the viscosity coefficient of NMP η is 1.7×10^{-3} Pa·s, the graphite flake average radius R is roughly estimated to be 1 μm, the graphite thickness h is approximately 7 nm, the laser beam intensity I is 100 W/cm^2, and the portion of fluid globe rotating together with the flake ξ is estimated to be 0.03. The value given by the model is in well agreement with the measured time 0.43 s (Fig. 3(b)). Since the formation of the "Wind Chime" is a collective behavior and a multi-process involving mechanical rotation, although its microscopic individual response is ultrafast (due to its electronic origin), the overall process behaves slowly.

Furthermore, we investigated the laser wavelength-dependence of the SSPM. Figure 4(a) shows the SSPM

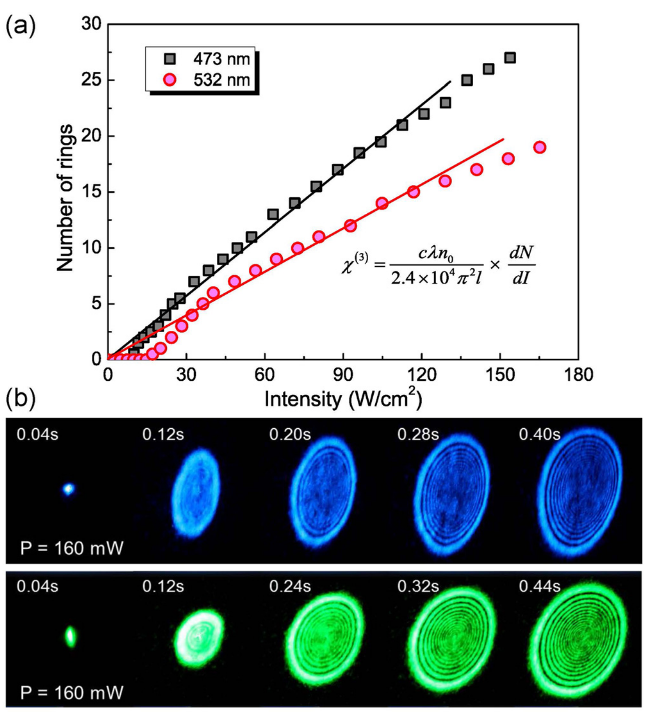

FIG. 3. (a) Intensity dependence of the ring number at different wavelength. The slope gives the $\chi^{(3)}$ value. (b) The time evolution of the SSPM ring formation processes at 473 nm and 532 nm, respectively, demonstrating the emergence of electron coherence as a collective behavior.

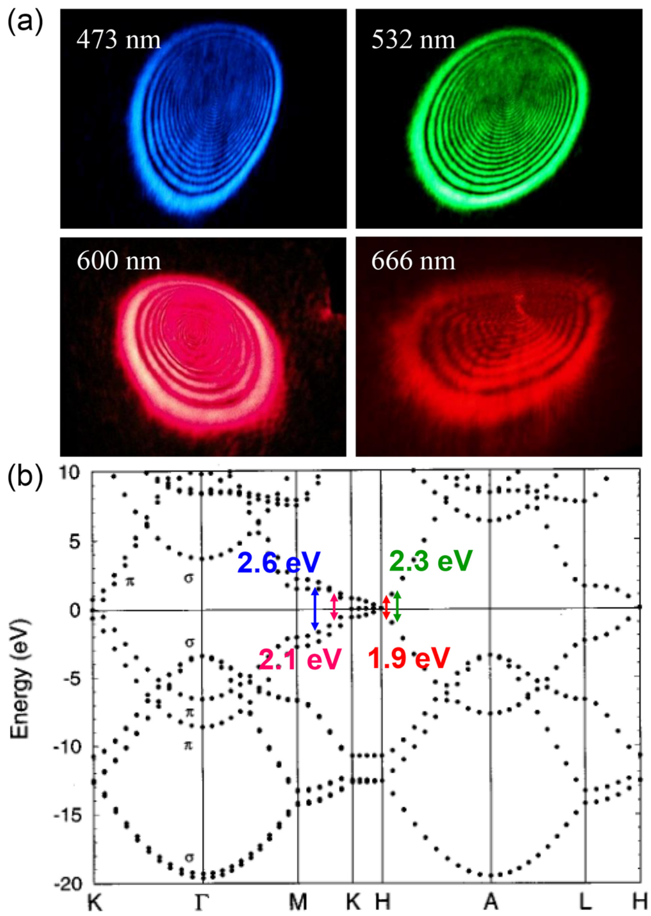

FIG. 4. (a) Photographs of the SSPM patterns at various laser wavelengths, illustrating the broadband property of SSPM in graphite. (b) Corresponding K-space quantum transitions for the SSPM processes in (a). The calculated electronic structure of graphite is adopted with permission from Boettger, Phys. Rev. B 55, 11202 (1997). Copyright 1997 American Physical Society. The modifications in (b), including the arrows drawn to energy scale, are marked with corresponding colors.

patterns at different wavelength excitations (with photon energies ranging from 1.9 eV to 2.6 eV). In Fig. 4(b), we adopt from Ref. 20 the calculated electronic structure of graphite to identify the corresponding K-space valence-to-conduction band quantum transition for the SSPM processes in Fig. 4(a). The colored arrows are marked to energy scale with corresponding light colors. This illustrates that $\chi^{(3)}$ values at different wavelengths are intrinsically determined by the electronic structure of the quantum materials.[6–8]

The diameter D of the outermost ring also increases linearly with intensity. However, unlike N, D is determined not only by n_2 but also by n_0.[6–8] For example, in Fig. 4(a), the ring numbers are not modified so N is a constant during the pattern deformation, manifesting a constant n_2. However, D is modified to become smaller for the upper half ring, which can only be due to the change in n_0. This occurs at the ring deformation process but not in the initial ring formation process (which is of electronic origin), and is explained as a thermal effect or gravitational effect.[6–8,33]

In conclusion, we have observed the SSPM of 3D graphite flakes. The third-order nonlinear optical susceptibility (for effective one-layer) $\chi^{(3)} = 2.2 \times 10^{-9}$ (esu) at 532 nm excitation and $\chi^{(3)} = 2.9 \times 10^{-9}$ (esu) at 473 nm excitation were measured, respectively. The time-dependent ring formation was recorded, revealing the laser-induced nonlocal electron coherence established among graphite flakes. The investigation of wavelength-dependent SSPM signifies its correlation to the electronic structure of the materials, which exhibits potentials for photonics applications of broadband graphite. Significantly, our finding that $\chi^{(3)}_{\mathrm{graphene}} > \chi^{(3)}_{\mathrm{graphite}} > \chi^{(3)}_{C_{60}}$ cannot be explained by a thermal effect explanation, thus, besides Ref. 6, further providing evidence for the electronic origin of SSPM.

This work was supported by the National Basic Research Program of China (2012CB821402, 2011CB606405, and 2012CB933002), the National Natural Science Foundation of China (11574383, 11274372, and 10974246), and the External Cooperation Program of Chinese Academy of Sciences (GJHZ1403).

[1]S. D. Durbin, S. M. Arakelian, and Y. R. Shen, Opt. Lett. 6, 411 (1981).
[2]K. S. Novoselov, A. K. Geim, S. V. Morozov, D. Jiang, Y. Zhang, S. V. Dubonos, I. V. Grigorieva, and A. A. Firsov, Science 306, 666 (2004).
[3]K. F. Mak, C. Lee, J. Hone, J. Shan, and T. F. Heinz, Phys. Rev. Lett. 105, 136805 (2010).
[4]K. S. Novoselov, D. Jiang, F. Schedin, T. J. Booth, V. V. Khotkevich, S. V. Morozov, and A. K. Geim, Proc. Natl. Acad. Sci. U. S. A. 102, 10451 (2005).
[5]X. D. Xu, W. Yao, D. Xiao, and T. F. Heinz, Nat. Phys. 10, 343 (2014).
[6]Y. L. Wu, Q. Wu, F. Sun, C. Cheng, S. Meng, and J. M. Zhao, Proc. Natl. Acad. Sci. U. S. A. 112, 11800 (2015).
[7]R. Wu, Y. L. Zhang, S. C. Yan, F. Bian, W. L. Wang, X. D. Bai, X. H. Lu, J. M. Zhao, and E. G. Wang, Nano Lett. 11, 5159 (2011).
[8]W. H. Wang, Y. L. Wu, Q. Wu, J. J. Hua, and J. M. Zhao, Sci. Rep. 6, 22072 (2016).
[9]Y. N. Han, W. J. Zhang, F. Z. Dong, Y. X. Xia, W. C. Zang, P. Yang, G. Gu, Y. W. Du, and D. Feng, Chin. Phys. Lett. 9, 647 (1992).
[10]L. Jensen and P. Th. V. Duijnen, Int. J. Quantum Chem. 102, 612 (2005).
[11]X. C. Liu, J. H. Si, B. H. Chang, G. Xu, Q. G. Yang, Z. W. Pan, S. S. Xie, and P. X. Ye, Appl. Phys. Lett. 74, 164 (1999).
[12]S. F. Wang, W. T. Huang, H. Yang, Q. H. Gong, Z. J. Shi, X. H. Zhou, D. Qiang, and Z. N. Gu, Chem. Phys. Lett. 320, 411 (2000).
[13]B. L. Wang, R. Wang, R. J. Liu, X. H. Lu, J. M. Zhao, and Z. Y. Li, Sci. Rep. 3, 2358 (2013).
[14]R. Wang, H. X. Yang, Y. B. Qin, B. Dong, J. Q. Li, and J. M. Zhao, J. Appl. Phys. 108, 073507 (2010).
[15]F. Sun, R. Wang, C. A. Leh, H. X. Yang, R. He, and J. M. Zhao, Sci. Rep. 4, 6429 (2014).
[16]S. F. Ge, X. F. Liu, X. F. Qiao, Q. S. Wang, Z. Xu, J. Qiu, P. H. Tan, J. M. Zhao, and D. Sun, Sci. Rep. 4, 5722 (2014).
[17]J. P. Prineas, W. J. Johnston, M. Yildirim, J. M. Zhao, and A. L. Smirl, Appl. Phys. Lett. 89, 241106 (2006).
[18]Z. L. Liu, Z. X. Mei, R. Wang, J. M. Zhao, H. L. Liang, Y. Guo, A. Y. Kuznetsov, and X. L. Du, J. Phys. D: Appl. Phys. 43, 285402 (2010).
[19]X. F. Han, Y. X. Weng, R. Wang, X. H. Chen, K. H. Luo, L.-A. Wu, and J. M. Zhao, Appl. Phys. Lett. 92, 151109 (2008).
[20]J. C. Boettger, Phys. Rev. B 55, 11202 (1997).
[21]B. Partoens and F. M. Peeters, Phys. Rev. B 74, 075404 (2006).
[22]A. Z. AlZahrani and G. P. Srivastava, J. Phys.: Condens. Matter 21, 495503 (2009).
[23]J. H. Wong, B. R. Wu, and M. F. Lin, Comput. Phys. Commun. 182, 77 (2011).
[24]A. C. Ferrari, Solid State Commun. 143, 47 (2007).
[25]A. Gupta, G. Chen, P. Joshi, S. Tadigadapa, and P. C. Eklund, Nano Lett. 6, 2667 (2006).
[26]Z. Q. Li, C. J. Lu, Z. P. Xia, Y. Zhou, and Z. Luo, Carbon 45, 1686 (2007).
[27]W. L. Mao, H. K. Mao, P. J. Eng, T. P. Trainor, M. Newville, C. C. Kao, D. L. Heinz, J. F. Shu, Y. Meng, and R. J. Hemley, Science 302, 425 (2003).
[28]E. Dervishi, Z. R. Li, F. Watanabe, A. Courte, A. Biswas, A. R. Biris, V. Saini, Y. Xu, and A. S. Biris, Chem. Mater. 21, 5491 (2009).

[29]Y. C. Tian, H. Tian, Y. L. Wu, L. L. Zhu, L. Q. Tao, W. Zhang, Y. Shu, D. Xie, Y. Yang, Z. Y. Wei, X. H. Lu, T. L. Ren, C. K. Shih, and J. M. Zhao, Sci. Rep. **5**, 10582 (2015).
[30]D. W. Wang, F. Li, Z. S. Wu, W. C. Ren, and H. M. Cheng, Electrochem. Commun. **11**, 1729 (2009).
[31]M. S. Dresselhaus and G. Dresselhaus, Adv. Phys. **51**, 1 (2002).
[32]See supplementary material at http://dx.doi.org/10.1063/1.4953827 for a general comparison with other carbon materials.
[33]W. Ji, W. Z. Chen, S. H. Lim, J. Y. Lin, and Z. X. Guo, Opt. Express **14**, 8958 (2006).